THE JOURNAL OF PHYSICAL CHEMISTRY C

pubs.acs.org/JPCC Article

Photophysical Properties of Zn-Alloyed $CsPbI_3$ Nanocrystals

Fuli Zhao, Junzi Li, Jiahao Yu, Zhihang Guo, Shuyu Xiao, Yang Gao, Ruikun Pan, Tingchao He,* and Rui Chen*

Cite This: *J. Phys. Chem. C* 2020, 124, 27169–27175 Read Online

ACCESS | Metrics & More | Article Recommendations

ABSTRACT: Deep-red luminescence emission makes $CsPbI_3$ nanocrystals (NCs) promising materials for various applications, but their use is limited in practice by instability in moist ambient environments. Incorporating Zn into $CsPbI_3$ NCs can help retain crystallinity and improve moisture resistance and device performance. However, a fundamental understanding of the photophysical properties of Zn-alloyed $CsPbI_3$ NCs remains incomplete. In this study, the differences in the photophysical properties of $CsPbI_3$ NCs and their Zn-alloyed counterparts ($CsPb_{0.8}Zn_{0.2}I_3$ NCs) are highlighted. Femtosecond transient absorption spectroscopy experiments show that the rate of carrier cooling is higher in $CsPb_{0.8}Zn_{0.2}I_3$ NCs than in $CsPbI_3$ NCs, whereas the two types of NCs exhibit similar Auger recombination lifetimes and biexcition binding energies. Our experimental results show more efficient multiphoton absorption by $CsPb_{0.8}Zn_{0.2}I_3$ NCs than by $CsPbI_3$ NCs. This result implies that Zn-alloyed $CsPbI_3$ NCs are promising materials for multiphoton-excited emission-relevant applications.

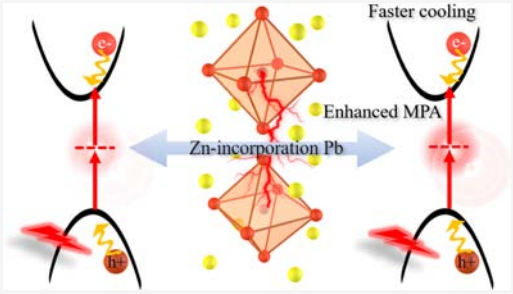

INTRODUCTION

All-inorganic perovskite nanocrystals (NCs) ($CsPbX_3$, X = Cl, Br, and I) are a new class of optoelectronic materials that have attracted significant interest for various superior properties, including a high photoluminescence quantum yield (PLQY), a tunable emission wavelength, defect tolerance, and solution processability.[1,2] Consequently, $CsPbX_3$ NCs exhibit considerable potential for various optoelectronic applications. Cubic (α)-phase $CsPbI_3$ NCs have the smallest band gap among various $CsPbX_3$ NCs and therefore are promising materials for applications in solar cells and red-emitting LEDs.[3,4] However, α-$CsPbI_3$ NCs suffer from photoinstability and easily undergo a phase transformation to a nonfunctional yellow orthorhombic (δ) phase shortly after preparation.[5,6]

Considerable effort has been expended to suppress photoluminescence (PL) loss and enhance the stability of red-emitting $CsPbI_3$ NCs. One general strategy to improve the phase stability of α-$CsPbI_3$ NCs is surface passivation using organic shells, such as 2,2′-iminodibenzoic acid (which acts as a bidentate passivation agent[7]) and A-site cation halide salts.[8] However, the common ligands that encapsulate NCs create an insulating layer that hinders carrier mobility and reduces device performance. The phase stability of cubic $CsPbI_3$ NCs can also be enhanced by replacing a few Pb^{2+} ions in the lattice with smaller cations to produce novel alloyed $CsPbI_3$ NCs.[9]

Although alloyed $CsPbI_3$ NCs exhibit considerable potential for various applications, there is yet no complete understanding of the fundamental photophysical properties of these materials, which is important for optimizing device performance and the development of design strategies for novel optoelectronic materials with tailored control over photophysical properties. For example, the mechanism and dynamics of hot carrier (HC) cooling in perovskite NCs are fundamentally important for the performance of solar cells and light-emitting diodes (LEDs).[10,11] Some applications of semiconductor NCs involve multiexciton states, including lasing, for which an understanding of the biexciton binding energy and Auger recombination (AR) processes are crucial.[12−16] In addition, studies on the multiphoton absorption (MPA) properties of halide perovskites are critically important for advancing applications.[17−20] Therefore, studies on the presently unknown ultrafast dynamics and MPA properties of Zn-alloyed perovskite NCs may facilitate applications in next-generation nonlinear photonic devices and in the biological sciences.

Inspired by the aforementioned applications, we used femtosecond transient absorption (fs-TA) spectroscopy to conduct a comparative study on the photophysical properties of bare $CsPbI_3$ NCs versus Zn-alloyed $CsPbI_3$ NCs, including the HC cooling time, the biexciton binding energy, and the biexciton AR lifetime. As heavy Zn incorporation [Zn-to-(Zn plus Pb) ratio > 0.25] can significantly destabilize Zn-alloyed $CsPbI_3$ NCs, a Zn-to-(Zn plus Pb) ratio of 0.2 was used, and

Received: September 14, 2020
Revised: October 25, 2020
Published: November 24, 2020

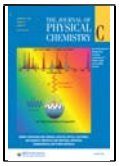

https://dx.doi.org/10.1021/acs.jpcc.0c08358
J. Phys. Chem. C 2020, 124, 27169−27175

the resultant $CsPb_{0.8}Zn_{0.2}I_3$ NCs were analyzed. The HC cooling time in $CsPb_{0.8}Zn_{0.2}I_3$ NCs was accelerated relative to that of bare $CsPbI_3$ NCs, whereas both types of NCs had similar biexciton binding energies and AR lifetimes. A significant result of this study was that the large transition oscillator strength of $CsPb_{0.8}Zn_{0.2}I_3$ NCs resulted in an enhanced MPA over that of bare $CsPbI_3$ NCs.

METHODS

Materials. $CsPbI_3$ and $CsPb_{0.8}Zn_{0.2}I_3$ NCs were synthesized using a previously reported hot injection method.[9] Briefly, the Cs-oleate precursor was prepared by placing cesium carbonate (Cs_2CO_3, 0.814 g), oleic acid (2.5 mL), and octadecene (30 mL) in a 100 mL flask. The mixture was degassed for 1 h at 120 °C and then heated to 150 °C under a nitrogen flow until a clear solution was obtained. Alloyed $CsPb_{0.8}Zn_{0.2}I_3$ NCs were synthesized by loading lead iodide (PbI_2, 0.376 mmol), zinc iodide (ZnI_2, 0.188 mmol), oleic acid (2 mL), oleylamine (2 mL), and 10 mL of octadecene into a 50 mL flask and degassing for 1 h at 120 °C. The solution was further heated to 170 °C under a nitrogen flow. Subsequently, a total of 1.5 mL of the Cs-oleate precursor was quickly injected into the solution, and after 5 s, the solution was immediately cooled to room temperature using an ice water bath. The crude solution was centrifuged at 5000 rpm for 10 min, the supernatant was discarded, and the precipitate was redispersed in toluene. The solution was recentrifuged at 10,000 rpm for 5 min, and the supernatant was discarded. Finally, the alloyed $CsPb_{0.8}Zn_{0.2}I_3$ NCs were redispersed in toluene for further characterization. Bare $CsPbI_3$ NCs were synthesized using the same procedure without ZnI_2 addition.

Characterizations. TEM specimens were prepared by transferring the NCs onto a holey carbon TEM grid. XPS patterns were obtained using a Bruker AXS D8. A PerkinElmer Lambda spectrophotometer was used to measure the linear absorption spectra. The PL spectrum and lifetime and PLQYs were measured using an Edinburgh FLSP 920 spectrophotometer equipped with a calibrated integrating sphere. During the lifetime measurement, the excitation wavelength was set at 375 nm (90 ps, 2 MHz).

Fs-TA Spectroscopy. A total of 800 nm pulses (100 fs, 1000 Hz) were first generated using a mode-locked Ti: sapphire laser (Spectra Physics). The beam was then split into two. One beam was used to generate a 350 nm excitation wavelength, and the second beam was passed through an optical delay line (with a time window of 3000 ps) and focused using a 2 mm thick sapphire to generate a white-light continuum (400−800 nm). The spectrum was dispersed on a cooled charge-coupled device.

Multiphoton-Excited PL Measurements. Multiphoton-excited PL spectra were obtained using pulses (100 fs, 1000 Hz) in wavelength ranges of 740−880 and 1500−2100 nm. The PL emission was collected perpendicular to the incoming excitation beam, and the signals were measured using a compact spectrometer (Ocean optics, HR4000).

Determination of MPA Cross-Sections. An open-aperture Z-scan setup that was constructed in-house was used to analyze the MPA cross-sections.[21] The measurements were carried out on well-stirred 1 mm cuvettes filled with perovskite NCs at a typical concentration of ~1×10^{-5} M.

EXPERIMENTAL RESULTS AND DISCUSSION

An XPS full-scan survey reveals that both types of NCs exhibited XPS peaks corresponding to Cs, Pb, I, O, and C (Figure 1a). In the high-resolution XPS spectra of Zn 2p

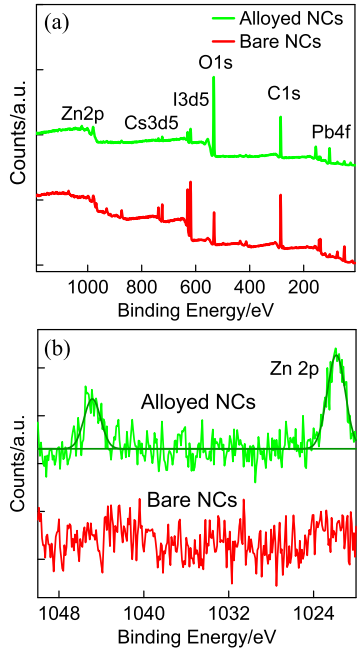

Figure 1. (a) XPS patterns of bare $CsPbI_3$ and alloyed $CsPb_{0.8}Zn_{0.2}I_3$ NCs and (b) high-resolution XPS spectra of Zn 2p.

(Figure 1b), the fitting peaks at 1021.8 and 1044.8 eV of $CsPb_{0.8}Zn_{0.2}I_3$ NCs are attributed to the Zn 2p signals of Zn^{2+}, which confirms the successful incorporation of zinc ions.

TEM images of the as-prepared perovskite NCs are shown in Figure 2a,b, clearly showing monodispersed cube-like NCs.

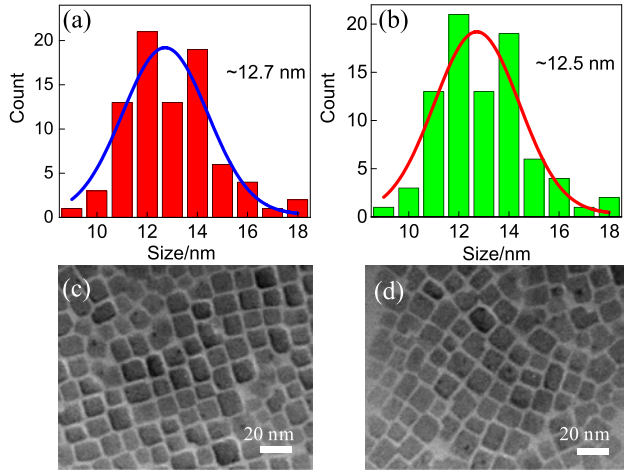

Figure 2. (a,b) TEM images of $CsPbI_3$ and $CsPb_{0.8}Zn_{0.2}I_3$ NCs and (c,d) size distribution histograms of $CsPbI_3$ and $CsPb_{0.8}Zn_{0.2}I_3$ NCs.

The corresponding size distribution histograms are presented in Figure 2c,d. The average edge lengths of bare $CsPbI_3$ and alloyed $CsPb_{0.8}Zn_{0.2}I_3$ NCs were estimated as 12.7 and 12.5 nm, respectively. Therefore, low Zn incorporation only slightly changed the size of the $CsPbI_3$ NCs.

https://dx.doi.org/10.1021/acs.jpcc.0c08358
J. Phys. Chem. C 2020, 124, 27169−27175

Figure 3a shows the absorption and PL spectra of the as-prepared perovskite NCs. Both the absorption and PL peaks of

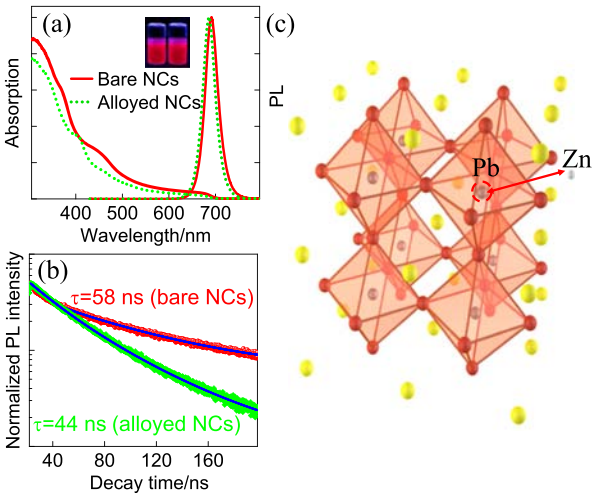

Figure 3. (a) Absorption and PL spectra of bare $CsPbI_3$ and alloyed $CsPb_{0.8}Zn_{0.2}I_3$ NCs: insets are photographs of perovskite NCs under UV light (365 nm) irradiation; (b) PL decay curves of perovskite NCs excited at 375 nm; and (c) crystal structure of alloyed $CsPb_{0.8}Zn_{0.2}I_3$ NCs.

the alloyed $CsPb_{0.8}Zn_{0.2}I_3$ NCs were shifted toward shorter wavelengths compared with bare $CsPbI_3$ NCs because of lattice contraction and a reduction in the NC size.[9] The PL wavelength peaks appeared at 691 nm for the $CsPbI_3$ NCs and 685 nm for the $CsPb_{0.8}Zn_{0.2}I_3$ NCs. The inset of Figure 3a shows that both the $CsPbI_3$ and $CsPb_{0.8}Zn_{0.2}I_3$ NCs exhibit bright-red emission under UV-light irradiation. The corresponding absolute PLQYs were determined to be 39.3 and 59.9%. The enhanced PLQY resulted from the low incorporation of zinc ions, indicating that fewer nonradiative channels were involved in the $CsPb_{0.8}Zn_{0.2}I_3$ NCs than in the $CsPbI_3$ NCs. Figure 3b shows that the average lifetime decreased from 58 ns for bare $CsPbI_3$ NCs to 44 ns for alloyed $CsPb_{0.8}Zn_{0.2}I_3$ NCs, which was consistent with results from the literature.[9] The crystal structure of alloyed $CsPb_{0.8}Zn_{0.2}I_3$ NCs is presented in Figure 3c.

The determination of the solution concentration of perovskite NCs is a prerequisite for a quantitative investigation of ultrafast dynamics and the MPA. Fs-TA spectroscopy has been proven to be an effective tool to determine the linear absorption cross-section (σ_{lin}) of novel synthesized materials,[22,23] wherein the following equation is used to fit the fs-TA spectrum for a long delay time

$$-A(I/I_0) = -A_{max}[1 - e^{-(I/I_0)\cdot\sigma_{lin}\cdot I_0}] \quad (1)$$

where $A(I/I_0)$ is the ground-state bleaching (GSB) signal amplitude of NCs at a long delay time as a function of the excitation intensity and I_0 is the minimum excitation intensity used in the fs-TA experiment.[22] Figure 4 shows the excitation intensity-dependent GSB amplitude at a 1 ns delay time for $CsPbI_3$ and $CsPb_{0.8}Zn_{0.2}I_3$ NCs excited at a 350 nm wavelength. Equation 1 was used to determine the σ_{lin} values at 350 nm as ~2.6×10^{-14} cm^2 for $CsPbI_3$ NCs and ~3.0×10^{-14} cm^2 for $CsPb_{0.8}Zn_{0.2}I_3$ NCs.

Next, we used fs-TA spectroscopy to study HC cooling dynamics in perovskite NCs (Figure 5). Cooling dynamics is

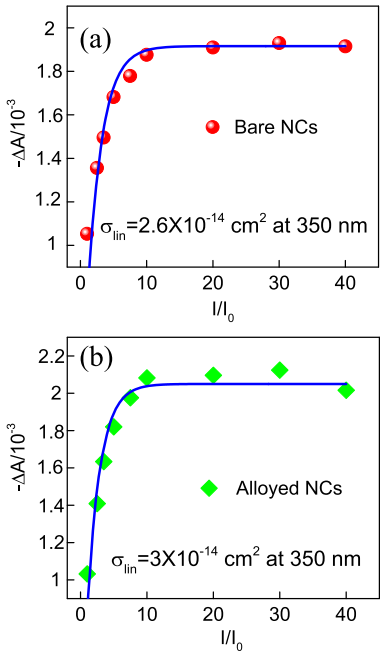

Figure 4. Excitation intensity-dependent GSB amplitude at 1 ns delay time for (a) $CsPbI_3$ NCs and (b) $CsPb_{0.8}Zn_{0.2}I_3$ NCs. Solid lines are theoretical fits using eq 1.

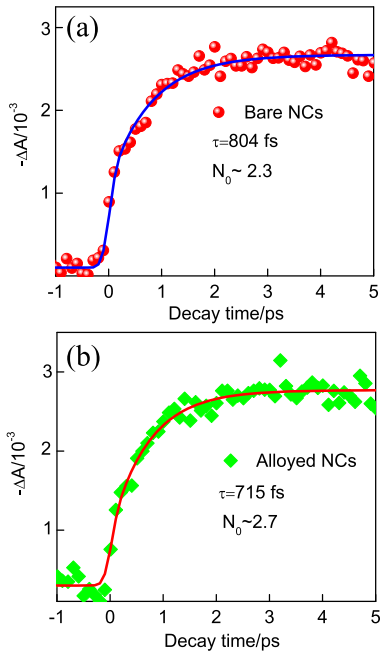

Figure 5. HC cooling processes for (a) $CsPbI_3$ NCs and (b) $CsPb_{0.8}Zn_{0.2}I_3$ NCs; corresponding HC cooling time values were obtained by fitting GSB extracted from spectral evolution of data on early ps time scales at 678 and 674 nm.

influenced by both the excitation energy and the carrier density.[23,24] Therefore, the same excitation wavelength of 350 nm and electron–hole pairs generated per NC (which was calculated as 2.5 using $\langle N_0 \rangle = j\sigma$, where j is the pump fluence) were chosen for both $CsPb_{0.8}Zn_{0.2}I_3$ and $CsPbI_3$ NCs to confirm the intrinsic influence of composition. HCs were found to relax faster in $CsPb_{0.8}Zn_{0.2}I_3$ NCs (~715 fs) than in $CsPbI_3$ NCs (~804 fs). Although fast HC cooling is

https://dx.doi.org/10.1021/acs.jpcc.0c08358
J. Phys. Chem. C 2020, 124, 27169−27175

detrimental for photovoltaic cell applications, this process in $CsPb_{0.8}Zn_{0.2}I_3$ NCs is favorable for applications such as LEDs.

The biexciton recombination lifetimes of NCs were determined by fs-TA spectroscopy. The pump wavelength was set at 350 nm for both $CsPbI_3$ and $CsPb_{0.8}Zn_{0.2}I_3$ NCs. Biexciton recombination dynamics can be analyzed by probing the kinetics of the GSB state.[24−27] Figure 6a,b shows the excitation intensity-dependent fs-TA kinetics probed at the GSB wavelengths of $CsPbI_3$ NCs (678 nm) and $CsPb_{0.8}Zn_{0.2}I_3$ (674 nm). Biexciton recombination caused the amplitude of the fast decay component to grow rapidly with the pump intensity. After subtraction according to the procedure described in ref 28, the biexciton recombination kinetics (which are plotted in Figure 6c) could be fitted by a single-exponential function. The time constants were determined as ~100 ps for both the $CsPbI_3$ and $CsPb_{0.8}Zn_{0.2}I_3$ NCs. As this value is much shorter than a quarter of the single-exciton lifetimes of $CsPbI_3$ and $CsPb_{0.8}Zn_{0.2}I_3$ NCs, the fast biexciton decay should be dominated by the nonradiative AR process.[28] In addition, almost the same AR lifetime for both types of perovskite NCs indicates comparable Coulombic interactions. Wu and co-workers proved that the biexciton AR lifetime of perovskite NCs can be influenced by the halide composition and size, which can be explained theoretically in terms of the combined effect of interband transition probabilities and the density of final states.[16] Therefore, the contributions of interband transition probabilities and the density of final states should be comparable for $CsPbI_3$ and $CsPb_{0.8}Zn_{0.2}I_3$ NCs.

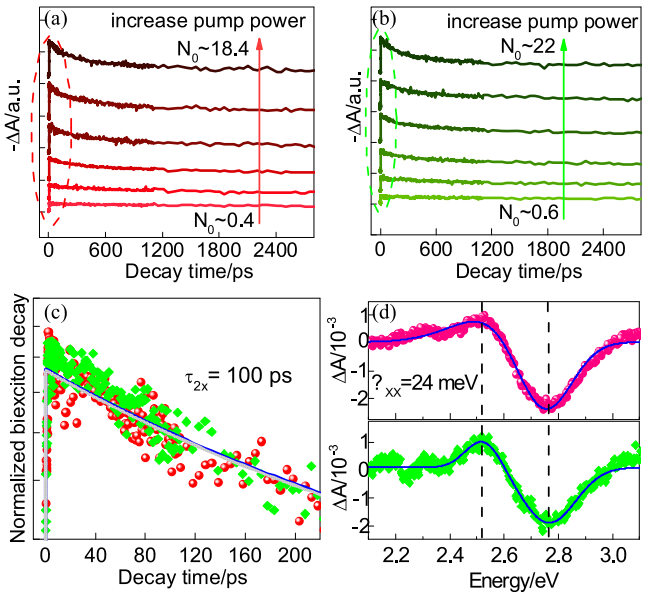

Figure 6. (a,b) Fs-TA kinetics probed at GSB wavelengths of 678 nm for $CsPbI_3$ NCs and 674 nm for $CsPbI_3$ NCs with varying pump intensities; (c) biexciton AR kinetics for perovskite NCs; and (d) Fs-TA spectra at 300 fs delay time for $CsPbI_3$ and $CsPb_{0.8}Zn_{0.2}I_3$ NCs. Solid lines represent global fits using eq 2.

The biexciton binding energies (Δ_{xx}) of NCs are significant parameters for the evaluation of the optical gain and can be obtained by fitting the fs-TA spectrum at an early delay time using the following equation[29]

$$A(E) = A_1 \exp\left[-\left(\frac{E - E_x - \Delta_{xx}}{w}\right)^2\right] - A_2 \exp\left[-\left(\frac{E - E_x}{w}\right)^2\right] \quad (2)$$

where A_1 and A_2 are the amplitudes of the photoinduced absorption and GSB signals, respectively. E_X and w are the

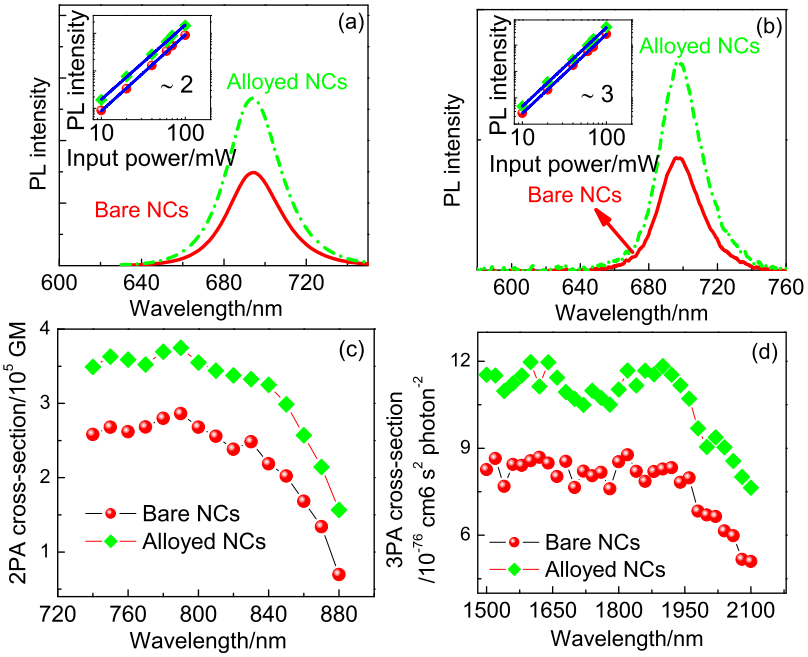

Figure 7. (a,b) Measured PL intensity of perovskite NCs at 800 nm (excitation power: 10 mW) and 1800 nm (excitation power: 30 mW), respectively. Insets: the excitation power-dependent PL intensity plotted on log scales at 800 and 1800 nm, respectively. The solid lines are fitting results, with indicated slopes. (c,d) Wavelength dispersion of 2PA and 3PA cross-sections of perovskite NCs.

https://dx.doi.org/10.1021/acs.jpcc.0c08358
J. Phys. Chem. C 2020, 124, 27169−27175

exciton energy and the half width measured for the optical absorption, respectively.

Figure 6d is a plot of the fs-TA spectra of NCs at a time delay of 300 fs. Almost the same Δ_{xx} value (~24 meV) is obtained from fitting the fs-TA spectra with eq 2 for both the $CsPbI_3$ and $CsPb_{0.8}Zn_{0.2}I_3$ NCs. This small value can be attributed to the weak-confinement regime for the two types of perovskite NCs.[30] Thus, low Zn incorporation into $CsPbI_3$ NCs will not marginally influence the biexciton binding energy of these NCs, which again suggests that the two types of perovskite NCs have comparable Coulombic interactions. The reduction in the HC cooling time without a change in the biexciton binding energy makes $CsPb_{0.8}Zn_{0.2}I_3$ NCs promising materials for lasing applications.

The UV−Vis linear absorption spectra of perovskite NCs indicate that two or three photons may be absorbed under fs pulse excitation in the 740−880 and 1500−2100 nm wavelength ranges. The MPA behavior was explored further by investigating the pumping intensity-dependent PL intensity (Figure 7a,b) to determine the number of photons absorbed in the excitation process.[31] The slopes (corresponding to the number of photons absorbed) were ~2 at 800 nm and ~3 at 1800 nm, clearly indicating the dominance of the two- and three-photon absorption (2PA and 3PA processes), respectively. Figure 7c shows the wavelength dispersion of the 2PA cross-section for $CsPbI_3$ and $CsPb_{0.8}Zn_{0.2}I_3$ NCs. The maximum 2PA cross-section of $CsPb_{0.8}Zn_{0.2}I_3$ NCs (~3.75×10^5 GM at 790 nm) was 1.3 times larger than that of $CsPbI_3$ NCs (~2.86×10^5 GM at 790 nm). We were encouraged by the large 2PA of these NCs and subsequently measured the wavelength dispersion of the 3PA cross-section (Figure 7b). Zn incorporation was also found to enhance the 3PA cross-section of $CsPbI_3$ NCs, with maximum values of ~8.77×10^{-76} cm^6 s^2 $photon^{-2}$ at 1820 nm for $CsPbI_3$ NCs and ~1.20×10^{-75} cm^6 s^2 $photon^{-2}$ at 1820 nm for $CsPb_{0.8}Zn_{0.2}I_3$ NCs. Clearly, low Zn incorporation can enhance both the 2PA and 3PA cross-sections of $CsPbI_3$ NCs, probably because redistribution of delocalized electrons is facilitated by the higher structural destabilization in $CsPb_{0.8}Zn_{0.2}I_3$ NCs than in $CsPbI_3$ NCs.[32] It should be stressed that there are few reports on the MPA of perovskite NCs across the NIR-III (1600−1870 nm) to NIR-IV (2100−2300 nm) biological regions.[19,33,34] Their maximum MPA cross-sections are several orders of magnitude larger than those of organic molecules, including unsymmetrical cyanostilbene derivatives (~6.0×10^{-80} cm^6 s^2 $photon^{-2}$ at 1110 nm)[35] and BODIPY dye (~0.93×10^{-80} cm^6 s^2 $photon^{-2}$ at 1600 nm).[36] Such a broad and strong 3PA process for alloyed $CsPb_{0.8}Zn_{0.2}I_3$ NCs offers significant advantages for deep-tissue bioimaging.

Although low Zn incorporation does not appear to significantly enhance the MPA cross-section of $CsPbI_3$ NCs, Zn-alloyed NCs offer other advantages. $CsPb_{0.8}Zn_{0.2}I_3$ NCs have a higher quantum yield than $CsPbI_3$ NCs. Consequently, the difference in the MPA action cross-sections between $CsPbI_3$ and $CsPb_{0.88}Zn_{0.12}$ NCs should be even more distinct than the corresponding difference in the MPA cross-sections. The maximum 2PA action cross-section of $CsPbI_3$ and $CsPb_{0.8}Zn_{0.2}I_3$ NCs can be estimated as ~1.03×10^5 and ~1.88×10^5 GM at 790 nm, respectively, whereas the corresponding values for the 3PA case are ~3.16×10^{-76} and ~6.0×10^{-76} cm^6 s^2 $photon^{-2}$ at 1820 nm. Compared to $CsPbI_3$ NCs, larger action cross-sections make $CsPb_{0.8}Zn_{0.2}I_3$ NCs more suitable for applications in MPA-based biological probes and emissive devices.

CONCLUSIONS

In summary, fs-TA spectroscopy was used to perform a comparative study of how Zn incorporation affects the ultrafast carrier dynamics of $CsPbI_3$ and $CsPb_{0.8}Zn_{0.2}I_3$ NCs. The results of the study show that Zn incorporation has a slight impact on the HC cooling process but almost no impact on the AR lifetime and biexciton binding energy. Note that $CsPb_{0.8}Zn_{0.2}I_3$ NCs exhibit larger MPA cross-sections and better stability than $CsPbI_3$ NCs and are therefore promising candidates for applications related to multiphoton-excited PL emission.

AUTHOR INFORMATION

Corresponding Authors

Tingchao He − *Key Laboratory of Optoelectronic Devices and Systems of Ministry of Education and Guangdong Province, College of Physics and Optoelectronic Engineering, Shenzhen University, Shenzhen 518060, P. R. China;* orcid.org/0000-0003-1040-0596; Email: tche@szu.edu.cn

Rui Chen − *Department of Electrical and Electronic Engineering, Southern University of Science and Technology, Shenzhen 518055, P. R. China;* orcid.org/0000-0002-0445-7847; Email: chenr@sustech.edu.cn

Authors

Fuli Zhao − *College of Arts and Science, Shanghai Dianji University, Shanghai 201306, P. R. China; Department of Electrical and Electronic Engineering, Southern University of Science and Technology, Shenzhen 518055, P. R. China*

Junzi Li − *Key Laboratory of Optoelectronic Devices and Systems of Ministry of Education and Guangdong Province, College of Physics and Optoelectronic Engineering, Shenzhen University, Shenzhen 518060, P. R. China*

Jiahao Yu − *Department of Electrical and Electronic Engineering, Southern University of Science and Technology, Shenzhen 518055, P. R. China*

Zhihang Guo − *Key Laboratory of Green Preparation and Application for Functional Materials, Ministry of Education, School of Materials Science and Engineering, Hubei University, Wuhan 430062, P. R. China*

Shuyu Xiao − *Key Laboratory of Optoelectronic Devices and Systems of Ministry of Education and Guangdong Province, College of Physics and Optoelectronic Engineering, Shenzhen University, Shenzhen 518060, P. R. China*

Yang Gao − *Key Laboratory of Optoelectronic Devices and Systems of Ministry of Education and Guangdong Province, College of Physics and Optoelectronic Engineering, Shenzhen University, Shenzhen 518060, P. R. China*

Ruikun Pan − *Key Laboratory of Green Preparation and Application for Functional Materials, Ministry of Education, School of Materials Science and Engineering, Hubei University, Wuhan 430062, P. R. China*

Complete contact information is available at: https://pubs.acs.org/10.1021/acs.jpcc.0c08358

Author Contributions

The manuscript was written through contributions of all authors. All authors have given approval to the final version of the manuscript.

https://dx.doi.org/10.1021/acs.jpcc.0c08358
J. Phys. Chem. C 2020, 124, 27169−27175

Notes

The authors declare no competing financial interest.

■ ACKNOWLEDGMENTS

We acknowledge financial support by the Guangdong Basic and Applied Basic Research Foundation (2019A1515012094), the Project of Department of Education of Guangdong Province (2018KTSCX19), and the Shenzhen Fundamental Research Project of Science and Technology (JCYJ20190808121211510).

■ REFERENCES

(1) Protesescu, L.; Yakunin, S.; Bodnarchuk, M. I.; Krieg, F.; Caputo, R.; Hendon, C. H.; Yang, R. X.; Walsh, A.; Kovalenko, M. V. Nanocrystals of Cesium Lead Halide Perovskites (CsPbX3, X = Cl, Br, and I): Novel Optoelectronic Materials Showing Bright Emission with Wide Color Gamut. *Nano Lett.* **2015**, *15*, 3692−3696.

(2) Song, J.; Li, J.; Li, X.; Xu, L.; Dong, Y.; Zeng, H. Quantum Dot Light-Emitting Diodes Based on Inorganic Perovskite Cesium Lead Halides (CsPbX3). *Adv. Mater.* **2015**, *27*, 7162−7167.

(3) Swarnkar, A.; Marshall, A. R.; Sanehira, E. M.; Chernomordik, B. D.; Moore, D. T.; Christians, J. A.; Chakrabarti, T.; Luther, J. M. Quantum dot-induced phase stabilization of -CsPbI3 perovskite for high-efficiency photovoltaics. *Science* **2016**, *354*, 92−95.

(4) Li, X.; Wu, Y.; Zhang, S.; Cai, B.; Gu, Y.; Song, J.; Zeng, H. CsPbX3Quantum Dots for Lighting and Displays: Room-Temperature Synthesis, Photoluminescence Superiorities, Underlying Origins and White Light-Emitting Diodes. *Adv. Funct. Mater.* **2016**, *26*, 2435−2445.

(5) Dutta, A.; Pradhan, N. Phase-Stable Red-Emitting CsPbI3 Nanocrystals: Successes and Challenges. *ACS Energy Lett.* **2019**, *4*, 709−719.

(6) Sutton, R. J.; Filip, M. R.; Haghighirad, A. A.; Sakai, N.; Wenger, B.; Giustino, F.; Snaith, H. J. Cubic or Orthorhombic? Revealing the Crystal Structure of Metastable Black-Phase CsPbI3 by Theory and Experiment. *ACS Energy Lett.* **2018**, *3*, 1787−1794.

(7) Pan, J.; Shang, Y.; Yin, J.; De Bastiani, M.; Peng, W.; Dursun, I.; Sinatra, L.; El-Zohry, A. M.; Hedhili, M. N.; Emwas, A.-H.; et al. Bidentate Ligand-Passivated CsPbI3 Perovskite Nanocrystals for Stable Near-Unity Photoluminescence Quantum Yield and Efficient Red Light-Emitting Diodes. *J. Am. Chem. Soc.* **2018**, *140*, 562−565.

(8) Dutta, A.; Pradhan, N. Phase-Stable Red-Emitting CsPbI3 Nanocrystals: Successes and Challenges. *ACS Energy Lett.* **2019**, *4*, 709−719.

(9) Shen, X.; Zhang, Y.; Kershaw, S. V.; Li, T.; Wang, C.; Zhang, X.; Wang, W.; Li, D.; Wang, Y.; Lu, M.; et al. Zn-Alloyed CsPbI3 Nanocrystals for Highly Efficient Perovskite Light-Emitting Devices. *Nano Lett.* **2019**, *19*, 1552−1559.

(10) Li, J.; Jing, Q.; Xiao, S.; Gao, Y.; Wang, Y.; Zhang, W.; Sun, X. W.; Wang, K.; He, T. Spectral dynamics and multiphoton absorption properties of all-inorganic perovskite nanorods. *J. Phys. Chem. Lett.* **2020**, *11*, 4817−4825.

(11) Fu, J.; Xu, Q.; Han, G.; Wu, B.; Huan, C.; Leek, M.; Sum, T. Hot carrier cooling mechanisms in halide perovskites. *Nat. Commun.* **2017**, *8*, 1300.

(12) Kambhampati, P. Unraveling the structure and dynamics of excitons in semiconductor quantum dots. *Acc. Chem. Res.* **2011**, *44*, 1−13.

(13) Kambhampati, P. Hot exciton relaxation dynamics in semiconductor quantum dots: radiationless transitions on the nanoscale. *J. Phys. Chem. C* **2011**, *115*, 22089−22109.

(14) Kambhampati, P. Multiexcitons in semiconductor nanocrystals: a platform for optoelectronics at high carrier concentration. *J. Phys. Chem. Lett.* **2012**, *3*, 1182−1190.

(15) Cui, M.; Qin, C.; Jiang, Y.; Yuan, M.; Xu, L.; Song, D.; Jiang, Y.; Liu, Y. Direct observation of competition between amplified spontaneous emission and auger recombination in quasi-two-dimensional perovskites. *J. Phys. Chem. Lett.* **2020**, *11*, 5734−5740.

(16) Li, Y.; Luo, X.; Ding, T.; Lu, X.; Wu, K. Size- and Halide-Dependent Auger Recombination in Lead Halide Perovskite Nanocrystals. *Angew. Chem., Int. Ed.* **2020**, *59*, 14292.

(17) Xu, J.; Li, X.; Xiong, J.; Yuan, C.; Semin, S.; Rasing, T.; Bu, X. H. Halide perovskites for nonlinear optics. *Adv. Mater.* **2020**, *32*, 1806736.

(18) Wang, Y.; Li, X.; Zhao, X.; Xiao, L.; Zeng, H.; Sun, H. Nonlinear absorption and low-threshold multiphoton pumped stimulated emission from all-Inorganic perovskite nanocrystals. *Nano Lett.* **2016**, *16*, 448−453.

(19) Chen, W.; Bhaumik, S.; Veldhuis, S.; Xing, G.; Xu, Q.; Gratzel, M.; Mhaisalkar, S.; Mathews, N.; Sum, T. Giant five-photon absorption from multidimensional core-shell halide perovskite colloidal nanocrystals. *Nat. Commun.* **2017**, *8*, 15198.

(20) Zhao, F.; Li, J.; Gao, X.; Qiu, X.; Lin, X.; He, T.; Chen, R. Comparison Studies of the Linear and Nonlinear Optical Properties of CsPbBrxI3-x Nanocrystals: The Influence of Dimensionality and Composition. *J. Phys. Chem. C* **2019**, *123*, 9538−9543.

(21) Sheik-Bahae, M.; Said, A. A.; Wei, T.-H.; Hagan, D. J.; Van Stryland, E. W. Sensitive measurement of optical nonlinearities using a single beam. *IEEE J. Quantum Electron.* **1990**, *26*, 760−769.

(22) Chen, J.; Žídek, K.; Chábera, P.; Liu, D.; Cheng, P.; Nuuttila, L.; Al-Marri, M. J.; Lehtivuori, H.; Messing, M. E.; Han, K.; et al. Size- and Wavelength-Dependent Two-Photon Absorption Cross-Section of CsPbBr3 Perovskite Quantum Dots. *J. Phys. Chem. Lett.* **2017**, *8*, 2316−2321.

(23) He, T.; Li, J.; Qiu, X.; Xiao, S.; Yin, C.; Lin, X. Highly Enhanced Normalized-Volume Multiphoton Absorption in CsPbBr3 2D Nanoplates. *Adv. Opt. Mater.* **2018**, *6*, 1800843.

(24) Chen, J.; Messing, M. E.; Zheng, K.; Pullerits, T. Cation-dependent hot carrier cooling in halide perovskite nanocrystals. *J. Am. Chem. Soc.* **2019**, *141*, 3532−3540.

(25) Shukla, A.; Kaur, G.; Babu, J. K.; Ghorai, N.; Goswami, T.; Kaur, A.; Ghosh, H. N. Effect of confinement on the exciton and biexciton dynamics in perovskite 2D-nanosheets and 3D-nanocrystals. *J. Phys. Chem. Lett.* **2020**, *11*, 6344−6352.

(26) Cong, M.; Yang, B.; Chen, J.; Hong, F.; Yang, S.; Deng, W.; Han, K. Carrier Multiplication and Hot-Carrier Cooling Dynamics in Quantum-Confined CsPbI3 Perovskite Nanocrystals. *J. Phys. Chem. Lett.* **2020**, *11*, 1921−1926.

(27) Makarov, N. S.; Guo, S.; Isaienko, O.; Liu, W.; Robel, I.; Klimov, V. I. Spectral and dynamical properties of single excitons, biexcitons, and trions in cesium-lead-halide perovskite quantum dots. *Nano Lett.* **2016**, *16*, 2349−2362.

(28) Klimov, V. I. Multicarrier interactions in semiconductor nanocrystals in relation to the phenomena of auger recombination and carrier multiplication. *Annu. Rev. Condens. Matter Phys.* **2014**, *5*, 285−316.

(29) Aneesh, J.; Swarnkar, A.; Kumar Ravi, V.; Sharma, R.; Nag, A.; Adarsh, K. V. Ultrafast Exciton Dynamics in Colloidal CsPbBr3 Perovskite Nanocrystals: Biexciton Effect and Auger Recombination. *J. Phys. Chem. C* **2017**, *121*, 4734−4739.

(30) Castañeda, J.; Nagamine, G.; Bonato, L.; Voznyy, O.; Hoogland, S.; Nogueira, A.; Sargent, E.; Brito-Cruz, C.; Padilha, L. Efficient biexciton interaction in perovskite quantum dots under weak and strong confinement. *ACS Nano* **2016**, *10*, 8603−8609.

(31) He, G. S.; Tan, L.-S.; Zheng, Q.; Prasad, P. N. Multiphoton absorbing materials: molecular designs, characterizations, and applications. *Chem. Rev.* **2008**, *108*, 1245−1330.

(32) Li, J.; Ren, C.; Qiu, X.; Lin, X.; Chen, R.; Yin, C.; He, T. Ultrafast optical nonlinearity of blue-emitting perovskite nanocrystals. *Photon. Res.* **2018**, *6*, 554−559.

(33) Shi, L.; Sordillo, L. A.; Rodríguez-Contreras, A.; Alfano, R. Transmission in near-infrared optical windows for deep brain imaging. *J. Biophot.* **2016**, *9*, 38−43.

(34) Li, J.; Zhao, F.; Xiao, S.; Cheng, J.; Qiu, X.; Lin, X.; Chen, R.; He, T. Giant two- to five-photon absorption in CsPbBr27I03 two-dimensional nanoplatelets. *Opt. Lett.* **2019**, *44*, 3873−3876.

https://dx.doi.org/10.1021/acs.jpcc.0c08358
J. Phys. Chem. C 2020, 124, 27169−27175

(35) Mandal, A. K.; Sreejith, S.; He, T.; Maji, S. K.; Wang, X.-J.; Ong, S. L.; Joseph, J.; Sun, H.; Zhao, Y. Three-photon-excited luminescence from unsymmetrical cyanostilbene aggregates: morphology tuning and targeted bioimaging. *ACS Nano* **2015**, *9*, 4796−4805.
(36) Ren, C.; Deng, X.; Hu, W.; Li, J.; Miao, X.; Xiao, S.; Liu, H.; Fan, Q.; Wang, K.; He, T. A near-infrared I emissive dye: toward the application of saturable absorber and multiphoton fluorescence microscopy in the deep-tissue imaging window. *Chem. Commun.* **2019**, *55*, 5111−5114.

https://dx.doi.org/10.1021/acs.jpcc.0c08358
J. Phys. Chem. C 2020, 124, 27169−27175